Catalysis Today 357 (2020) 583–589

Contents lists available at ScienceDirect

Catalysis Today

journal homepage: www.elsevier.com/locate/cattod

Review

# Flexible syngas production using a $La_2Zr_{2-x}Ni_xO_{7-}\delta$ pyrochlore-double perovskite catalyst: Towards a direct route for gas phase $CO_2$ recycling

E. le Saché[a,*], L. Pastor-Pérez[a], V. Garcilaso[b], D.J. Watson[c], M.A. Centeno[b], J.A. Odriozola[b], T.R. Reina[a,*]

[a] Department of Chemical and Process Engineering, University of Surrey, Guildford, GU2 7XH, United Kingdom
[b] Departamento de Química Inorgánica, Universidad de Sevilla, Instituto de Ciencias de Materiales de Sevilla Centro mixto US-CSIC Avda. Américo Vespucio 49, 41092 Seville, Spain
[c] Department of Chemistry, University of Surrey, Guildford, GU2 7XH, United Kingdom

ARTICLE INFO

*Keywords:*
Pyrochlore
Bi-reforming of methane
Dry reforming of methane
Ni catalyst

ABSTRACT

The bi-reforming of methane (BRM) has the advantage of utilising greenhouse gases and producing $H_2$ rich syngas. In this work Ni stabilised in a pyrochlore-double perovskite structure is reported as a viable catalyst for both Dry Reforming of Methane (DRM) and BRM. A 10 wt.% Ni-doped $La_2Zr_2O_7$ pyrochlore catalyst was synthesised, characterised and tested under both reaction conditions and its performance was compared to a supported $Ni/La_2Zr_2O_7$. In particular the effect of steam addition is investigated revealing that steam increases the $H_2$ content in the syngas but limits reactants conversions. The effect of temperature, space velocity and time on stream was studied under BRM conditions and brought out the performance of the material in terms of activity and stability. No deactivation was observed, in fact the addition of steam helped to mitigate carbon deposition. Small and well dispersed Ni clusters, possibly resulting from the progressive exsolution of Ni from the mixed oxide structure could explain the enhanced performance of the catalyst.

## 1. Introduction

Carbon dioxide is the most abundant greenhouse gas and is mainly responsible for the observed global warming. It is the main product of total combustion in power plants and its concentration in the atmosphere has risen considerably since the beginning of the industrial era. In fact, $CO_2$ emissions related to energy grew by 1.4% in 2017, with a record level of 32.5 gigatonnes (Gt) according to the International Energy Agency [1]. Today, $CO_2$ recycling is under increased scrutiny as an alternative to the carbon capture and storage strategy to help $CO_2$ mitigation [2,3]. Carbon dioxide contributes to the synthesis of various higher value chemicals through organic carboxylation reactions leading to chemicals like urea, carboxylic acids, and isocyanates among others [2]. Another route to valuable chemicals is through the formation of syngas followed by further conversion processes such as the Fischer-Tropsch synthesis (FTS) that produces a variety of hydrocarbon fractions. The direct synthesis of methanol from syngas requires a $H_2/CO$ ratio of about 2 [4], where the hydroformylation process needs a $H_2/CO$ ratio of 1. On the other hand, the FTS usually uses a $H_2/CO$ syngas ratio of 2 but would benefit from a higher selectivity towards long-chain hydrocarbons with lower $H_2/CO$ ratios [5]. The most commonly used technology to produce syngas is the Steam Reforming of Methane (SRM, Eq. 1) producing a hydrogen rich syngas with a $H_2/CO$ ratio of about 3. The dry reforming of methane (DRM, Eq. 2) on the other hand, uses $CO_2$ as oxidant and leads to a syngas $H_2/CO$ mixture ratio of a maximum of 1. DRM has the advantage of utilising two of the most abundant greenhouse gases and hence has been increasingly investigated as a $CO_2$ recycling strategy [6,7]. Because the syngas produced by DRM is too poor in $H_2$ to be fed to a FT unit, bi-reforming of methane (BRM, Eq. 3) combining SRM and DRM is proposed to tune the syngas composition.

$$\text{SRM: } CH_4 + H_2O \rightleftharpoons CO + 3H_2 \quad (1)$$

$$\text{DRM: } CO_2 + CH_4 \rightleftharpoons 2CO + 2H_2 \quad (2)$$

$$\text{BRM: } 3CH_4 + CO_2 + 2H_2O \rightleftharpoons 4CO + 8H_2 \quad (3)$$

BRM is also advantageous in terms of biogas upgrading [8]. The composition of biogas produced through anaerobic digestion varies depending of the source and type of waste used, but consists mainly of $CH_4$, $CO_2$, $O_2$, $H_2O$ and impurities which can, after purification treatments, be used in a BRM unit.

* Corresponding authors.
*E-mail addresses:* e.lesache@surrey.ac.uk (E. le Saché), t.ramirezreina@surrey.ac.uk (T.R. Reina).

https://doi.org/10.1016/j.cattod.2019.05.039
Received 22 October 2018; Received in revised form 13 May 2019; Accepted 17 May 2019
Available online 22 May 2019

Reforming processes require high reaction temperatures to reach full reactant conversions but when exposed to such temperatures, typical metal supported on oxides catalysts are subject to deactivation due to sintering of the active phase [9,10]. Coke formation is also a major cause of deactivation due to several side reactions producing carbon such as the Boudouard reaction, $CH_4$ decomposition, CO reduction and $CO_2$ reduction [11–13]. Noble metals such as Rh, Ru, Pd and Pt have shown great catalytic activity and coke resistance, however for applications in large scale industrial processes low cost transition metals are preferred. Extensive research has been conducted in the recent years using Ni catalysts. They are low cost and exhibit good performance for reforming but suffer from severe deactivation. Stabilising Ni is essential to prevent sintering and at the same time to reducing carbon formation by preserving small Ni particles. The use of materials such as hexaaluminates, fluorites, perovskites and pyrochlores have been investigated for this purpose in reforming reactions [14–19]. Pyrochlores are mixed oxides of general formula $A_2B_2O_7$. The A-site represents a large trivalent cation, typically a rare-earth metal such as La and the B-site is occupied by a tetravalent cation of smaller diameter, typically a transition metal such as Zr [20]. They are benefit from high thermal stability and high oxygen mobility which makes them suitable candidates for high temperature operations and coke resistance [17]. For this reason, pyrochlores have been previously investigated, in particular in the steam reforming reactions. Ma et al. demonstrated that Ni supported on $La_2Zr_2O_7$ had superior activity to Ni supported on $La_2Sn_2O_7$ or γ-$Al_2O_3$ due to the large amount of $La_2O_2CO_3$ formed, effectively suppressing coke formation [18]. Zhang et al. supported Ni on various $Ln_2Zr_2O_7$ supports with different degrees of order, from pyrochlore to defective fluorites. The amount of oxygen vacancies and therefore mobility was key to mitigate carbon deposition [17]. Substitution of Ni in the B site of a pyrochlore has also shown promising activity in reforming reactions [21–24]. Previous work in our group showed that the substitution of 10 wt.% Ni on the B site of a $La_2Zr_2O_7$ pyrochlore led to a very active, stable and carbon resistant catalyst for DRM [25,26]. However the syngas obtained through DRM had a $H_2$/CO ratio of maximum 0.8 which limits its applicability for further chemical upgrading. With the purpose of tuning the $H_2$/CO ratio of the syngas produced by a stable DRM pyrochlore catalyst, a 10 wt.% Ni doped $La_2Zr_2O_7$ catalyst was tested under different sets of conditions, including BRM and compared to a supported 10 wt.% Ni on $La_2Zr_2O_7$ catalyst. The effect of temperature, space velocity and water content in the feed stream were studied as well as the catalyst stability and coke resistance. The studies show promising results for flexible syngas production.

## 2. Experimental

### 2.1. Catalyst preparation

The pyrochlore based materials were prepared using a modified citrate method described elsewhere [25]. Lanthanum nitrate [$La(NO_3)_3{\cdot}6H_2O$], nickel nitrate [$Ni(NO_3)_2{\cdot}6H_2O$], and zirconium nitrate [$ZrO(NO_3)_2{\cdot}6H_2O$] provided by Sigma-Aldrich were used as precursors. The necessary amount of each precursor was dissolved in deionized water and then mixed with a citric acid (CA) solution using a CA:metal molar ratio of 0.6:1. The solution was stirred and concentrated in a rotary evaporator. The resulting mixture was dried for 12 h at 100 °C prior combustion at 200 °C. The final powders were calcined at 1000 °C for 8 h to insure phase transition to pyrochlore. Ni was impregnated on the prepared un-doped pyrochlore using an incipient wetness method. [$Ni(NO_3)_2{\cdot}6H_2O$] was dissolved in ethanol and mixed to the support. The solvent was removed in a rotary evaporated and the resulting powder was dried for 12 h at 100 °C before calcination at 500 °C for 4 h. The doped catalyst will be referred as LNZ10 and the supported catalyst as Ni/LZ.

### 2.2. Catalysts characterisation

The textural properties of the material were determined by nitrogen adsorption-desorption measurements at −196 °C in an AUTOSORB-6 fully automated manometric equipment. The sample was degassed under vacuum at 250 °C for 4 h before each measurement. The BET equation was applied to estimate the specific surface area whilst pore-size distributions were determined using the Barett–Joyner–Halenda (BJH) method.

X-ray diffraction (XRD) analysis was conducted on fresh, reduced and used catalysts using an X'Pert Pro Powder Diffractometer by PANalytical. The 2θ angle was increased by 0.05° every 240 s over a range of 20–80 °. Diffraction patterns were recorded at 30 mA and 40 kV, using Cu Kα radiation (λ = 0.154 nm).

Temperature programmed reduction with hydrogen (TPR) analysis was carried out on the calcined catalyst in a U-shaped quartz reactor. A 50 mg sample was heated to 900 °C at a rate of 10 °C $min^{-1}$ in a flow of 50 mL $min^{-1}$ of 5% $H_2$ in Ar. A $CO_2$-ethanol trap was used to condense the gaseous products, mostly water, before the on stream thermal conductivity detector (TCD). The $H_2$ uptake was quantified by comparison with the hydrogen consumption of a CuO reference sample.

Temperature programmed oxidation (TPO) was conducted in a U-shaped quartz reactor coupled to a PFEIFFER Vacuum PrismaPlus mass spectrometer. Samples were heated up to 900 °C at a rate of 10 °C $min^{-1}$ in a flow of 50 mL $min^{-1}$ (5% $O_2$, 95% He).

Raman spectroscopy measurements were performed on a Thermo Scientific DXR Raman Microscope using a green laser (λ = 532 nm, maximum power 10 mW) with a spot diameter of 0.7 μm and a pinhole aperture of 50 μm. A diffraction grating of 900 grooves $mm^{-1}$, a CCD detector and a 50× objective were used.

### 2.3. Catalytic behaviour

Catalytic activity tests were performed in a computerised commercial Microactivity Reference catalytic reactor (PID Eng&Tech), employing a tubular quartz reactor of 9 mm internal diameter. The catalyst was sieved and the 100–200 μm fraction was used for testing, diluted with quartz to achieve a catalytic bed of 0.32 $cm^3$. Water was injected into the system by an HPLC pump (Gilson) before being vaporized and mixed with the gas stream before entering the reactor. The composition of the outlet of the reactor was followed by on-line gas chromatography using a MicroGC (Varian 4900) equipped with Porapak Q and MS-5A columns. Prior to reaction, the catalyst was reduced for 1 h at 650 °C in $H_2$ (10%, v/v in $N_2$). The gas composition was set to $CH_4/CO_2/H_2O/N_2$: 1/1/1/1 to achieve Weight Hourly Space Velocity (WHSV) from 20 to 60 $L.g^{-1}.h^{-1}$.

The effect of water partial pressure variation on the catalytic activity was also studied at 700 °C. In these experiments, the total flow was kept constant using $N_2$ to maintain the WHSV at 60 $L.g^{-1}.h^{-1}$. The feed composition was 25% $CH_4$ and 25% $CO_2$ while the water concentration was modified taking values of 15%, 25% and 35% (v/v).

### 2.4. Thermodynamic simulations

ChemStations' ChemCad software package was used to calculate the thermodynamic equilibrium fractions for both DRM and BRM reactions over a range of temperatures. The Soave-Redlich-Kwong equation of state was used in a Gibbs reactor. Material flows into the reactor are identical to those intended to be used for experimentation.

## 3. Results and discussion

### 3.1. X-Ray diffraction (XRD)

The XRD profiles of the freshly prepared catalysts are shown in Fig. 1. The LNZ10 sample presents the characteristic diffraction features

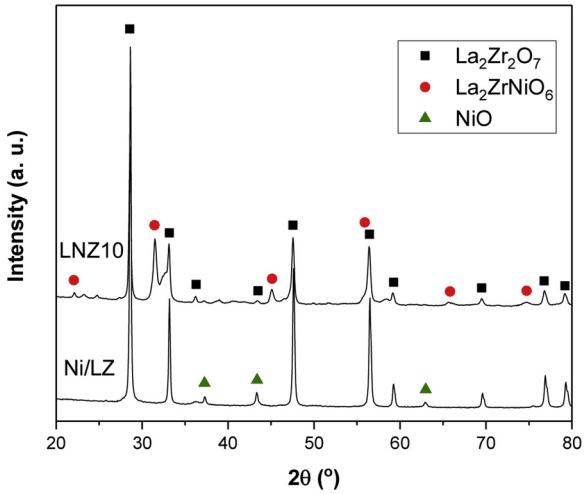


**Fig. 1.** XRD patterns of fresh Ni/LZ and LNZ10.

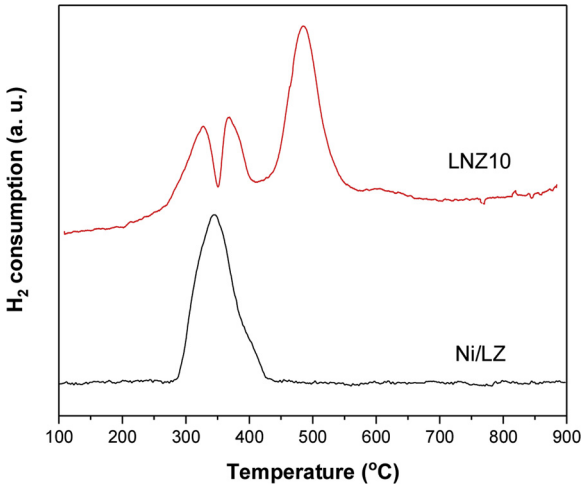


**Fig. 2.** TPR profile of Ni/LZ and LNZ10.

of two different phases. First, a $La_2Zr_2O_7$ pyrochlore phase (JCPDS Card No. 01-73-0444) was identified, the superstructure peaks (331) and (551) at 36.2° and 43.5° respectively, indicates that the phase transition between fluorite and pyrochlore was achieved [27–29]. These two diffraction peaks, low in intensity, correspond to the ordering of the cations (and anions) in the pyrochlore structure. This was confirmed by Raman analysis (Figure S2) where 5 peaks attributed the pyrochlore phase can be observed. Indeed the group theory predicts six Raman active modes ($A_{1g} + E_g + 4\ F_{2g}$) for the pyrochlore structure (Fd3m) and only one Raman mode ($F_{2g}$) for the fluorite structure (Fm3m). Here, five peaks corresponding to the pyrochlore-type structured lanthanum zirconate are visible in agreement with the XRD results. The intense Raman peak at 280 $cm^{-1}$ is the $E_g$ mode associated to O-Zr-O bending vibrations and two $F_{2g}$ modes at 492 and 391 $cm^{-1}$ are associated to Zr-O and La-O bond stretching with bending vibrations. The $A_{1g}$ mode at 530 $cm^{-1}$ corresponds to Zr-$O_6$ bending vibrations and the peak at 680 $cm^{-1}$ is assigned to the dopant –$O_6$ symmetrical stretch in the pyrochlore phase [30]. Second, two diffraction peaks at 31.5 and 45.1° indicate the presence of a $La_2NiZrO_6$ rhombohedral double perovskite oxide phase (JCPDS Card No. 00-044-0624). The Ni loading used here is above of the maximum substitution limit of the pyrochlore structure in agreement with Haynes et al. findings [31], leading to the formation of this additional phase. No characteristic diffraction peaks of individual $La_2O_3$ or $ZrO_2$ oxides are observed suggesting a complete incorporation of $La_2O_3$ and $ZrO_2$ into the pyrochlore and double perovskite structures. Since no peaks attributed to Ni or $NiO_x$ species are detected, Ni is either fully incorporated into the mixed structures or some individual Ni particles are formed outside of the bulk inorganic lattice but are sufficiently small and well dispersed not to be detected by XRD. The Ni/LZ sample on the other hand presents the typical diffraction peaks of NiO additionally to the $La_2Zr_2O_7$ pyrochlore phase. The $La_2NiZrO_6$ rhombohedral double perovskite oxide phase was not formed on the supported catalyst since this phase requires calcination temperatures ≥ 800 °C to be formed [31].

### 3.2. Reducibility: $H_2$-TPR

In order to obtain information about the reduction behaviour and interactions among the active species of the as-prepared catalysts, temperature-programmed reduction treatment were performed and the resulting $H_2$ consumption profile are shown in Fig. 2. The $La_2Zr_2O_7$ pyrochlore alone is not reducible [18,26] therefore $NiO_x$ species are responsible for any $H_2$ consumption in the catalysts [17,18]. Four reduction processes can be distinguished in the doped catalyst. First, easily accessible $NiO_x$ particles located on the outer layer of the catalyst are reduced at 330 °C. Their weak interactions with the bulk of the catalyst facilitate their reducibility [17,31]. The second reduction process at 370 °C is attributed to $NiO_x$ exsolved from the pyrochlore structure. Those particles are interacting with the $La_2Zr_2O_7$ pyrochlore and are therefore reduced at higher temperature [26]. The temperature peak at 485 °C corresponds to most of the $H_2$ uptake and is probably due to the reduction of $La_2NiZrO_6$ as observed by Haynes et al. [31]. The fourth reduction process at 600 °C could correspond to Ni exsolved from the pyrochlore structure and still strongly interacting with the pyrochlore. Overall the hydrogen uptake of the doped catalyst was 1.49 $mmol/g_{cat}$ which corresponds to the reduction of 69% of the Ni content of the catalyst. This suggests that some $Ni^{2+}$ remains under the double perovskite phase and inside the pyrochlore structure in fair agreement with the X-Ray diffraction results. Indeed, the XRD profile of the reduced catalyst shown in Fig. 7 still presents the characteristic pattern of the double perovskite phase. The supported catalyst on the other hand only presents two reduction processes. The peak at 345 °C corresponds to the reduction of large NiO particles in loose contact with the support and the second process at 400 °C is attributed to the reduction of NiO clusters in intimate contact with the pyrochlore [17].

### 3.3. Catalytic activity

#### 3.3.1. Stability test

The performance of the catalysts were tested under DRM and BRM conditions at 700 °C for a period of 24 h. The $CH_4$ and $CO_2$ conversions under both reaction conditions are shown in Fig. 3. Under DRM conditions, the doped pyrochlore exhibits excellent catalytic activity with $CH_4$ and $CO_2$ conversions of 87% and 90% respectively, reaching thermodynamics equilibrium. However, when 25% steam is introduced into the system, the conversions decrease to 54% for $CH_4$ and 39% for $CO_2$. The latter is a consequence of the thermodynamic constraints when DRM and BRM are coupled and also reflects the increased competition of both reactants with the new reactant (water) to reach the active sites of the catalysts. Thermodynamics predict a methane conversion of 92% and a carbon dioxide conversion of 47%. The lower performance of the doped catalyst, in particular in terms of methane conversion may be attributed to the reduced activation of $H_2O$ on the pyrochlore. In both scenarios, the doped catalyst stabilises very rapidly and shows no deactivation over the time frame of the experiments. On the other hand, the supported catalyst deactivates rapidly, emphasizing the Ni stabilisation induced by the doping strategy. In dry conditions the conversion of $CO_2$ is slightly larger than $CH_4$ likely due to the occurrence of the reverse water gas shift reaction (RWGS), consuming some of the carbon dioxide as reported elsewhere [32]. On the other hand, under BRM conditions, $CH_4$ conversion is largely above the one of

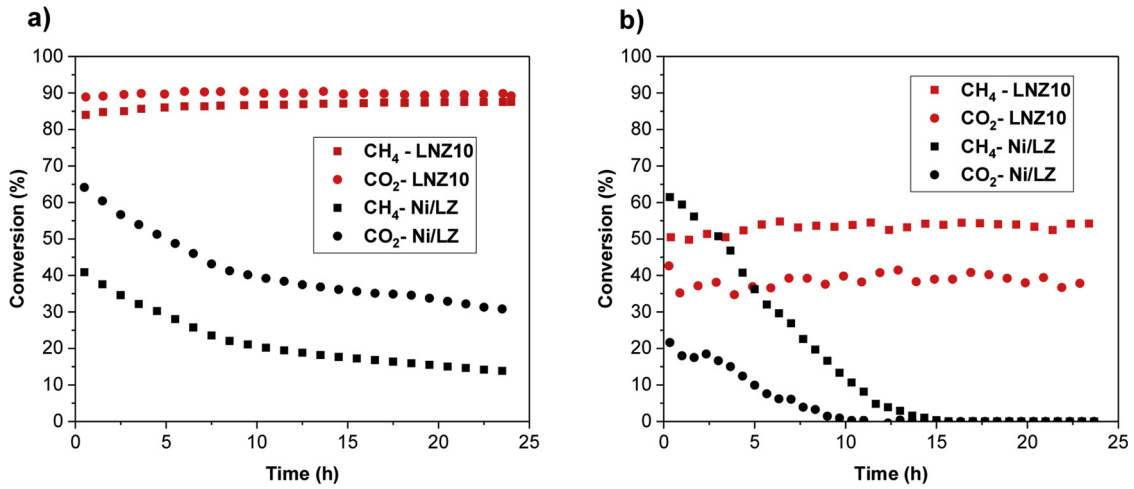


**Fig. 3.** Stability test performed on LNZ10 and Ni/LZ under a) DRM ($CH_4/CO_2/H_2O$: 1/1/0) and b) BRM ($CH_4/CO_2/H_2O$: 1/1/1) at P = 1 atm, WHSV = 30 $L.g^{-1}.h^{-1}$ and T = 700 °C.

$CO_2$. When steam is introduced, RWGS is no longer favoured and in turn SMR and forward WGS occur, therefore consuming more methane and increasing the $H_2/CO$ ratio.

### 3.3.2. Effect of water addition

The Ni-doped pyrochlore catalyst showed great performance in terms of activity and stability for both DRM and BRM. In order to tune the $H_2/CO$ ratio for downstream processes, the effect of steam addition in the feed stream was studied. The catalytic activity of the catalyst in terms of $CH_4$ and $CO_2$ conversions and $H_2/CO$ ratio as a function of water content is shown in Fig. 4. The performance of the catalyst was tested at relatively high space velocity (60 $L.g^{-1}.h^{-1}$) due to equipment limitations. As expected, the $H_2/CO$ ratio of the products increases greatly as the water content increases. DRM produces a syngas of $H_2/CO$ = 0.7 but, by introducing 35% steam, this ratio can be increased to 2.5. For an FT unit or methanol production, a quantity of 30% water would be necessary to obtain a $H_2$ rich syngas or metgas of $H_2/CO$ = 2. It seems however that the improvement in selectivity is made at the expense of conversion. Indeed, as more water is introduced the reactant conversion decreases. Water may promote the SMR reaction but overall, the catalytic activity of the pyrochlore catalyst decreases. Thermodynamically, the addition of water should lead to larger $CH_4$ conversion but a reduced $CO_2$ conversion. The observed decrease in both conversions is possibly due to a change in the kinetics of the reaction induced by water introduction. To the best of our knowledge, no kinetic or mechanistic study has been conducted on BRM to date using a comparable reactants mixture. However, SMR kinetics have been studied. Various studies in the literature have claimed a negative order of steam for SMR [33,34]. The dependence of steam on the rate of reaction can be due to the competition between $CH_4$ and $H_2O$ on the catalyst active sites as previously reported elsewhere and in good agreement with our trends [35].

### 3.3.3. Space velocity effect

Space velocity is a major parameter to consider for scaling up. It determines the volume of the reforming unit and the amount of catalyst needed. The space velocity effect was investigated under BRM conditions with 25% of steam and the results are shown in Fig. 5. Overall conversions of $CH_4$ and $CO_2$ decrease by increasing the space velocity, although the selectivity remains unchanged. At high space velocity, conversions are far from equilibrium values. However, when the space velocity is decreased to 20 $L.g^{-1}.h^{-1}$, $CO_2$ conversion nearly reaches the thermodynamic value. $CH_4$ on the other hand seems to be more affected by WHSV as a more significant decrease in conversion is observed when WHSV is increased. This observation actually reflects the fact that methane activation is the rate limiting step for this reaction [33] and therefore the conversion of this reactant is very sensitive to the operation conditions and the catalysts choice. In any case the fact that our catalyst can maintain a $H_2/CO$ ratio of over 1.5 (very close to the equilibrium limit) is a commendable achievement for the pyrochlore-

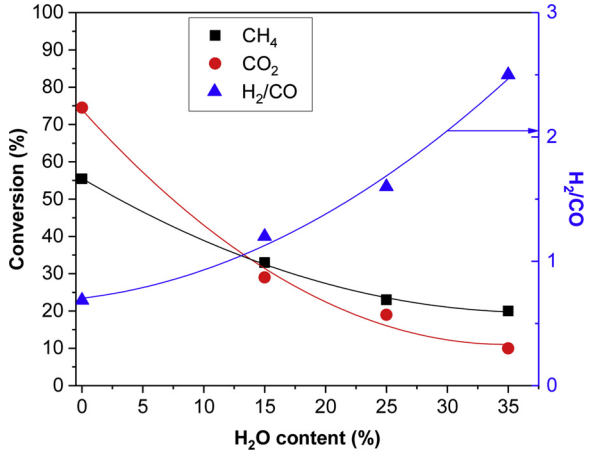


**Fig. 4.** Water content effect on $CH_4$ and $CO_2$ conversions and $H_2/CO$ ratio ($CH_4/CO_2$:1, P = 1 atm, T = 700 °C, WHSV = 60 $L.g^{-1}.h^{-1}$).

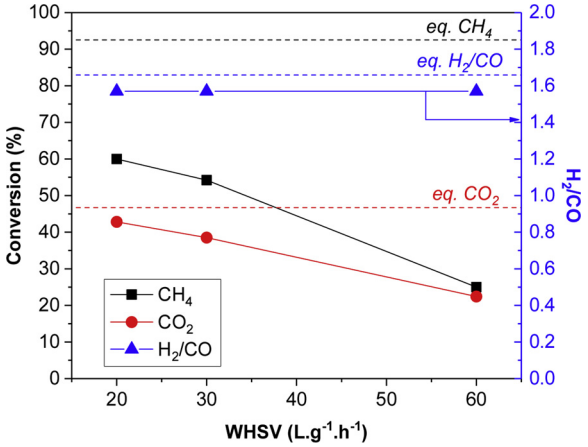


**Fig. 5.** Space velocity effect on $H_2/CO$ ratio and $CH_4$ and $CO_2$ conversion (P = 1 atm, $CH_4/CO_2/H_2O$: 1/1/1, T = 700 °C).

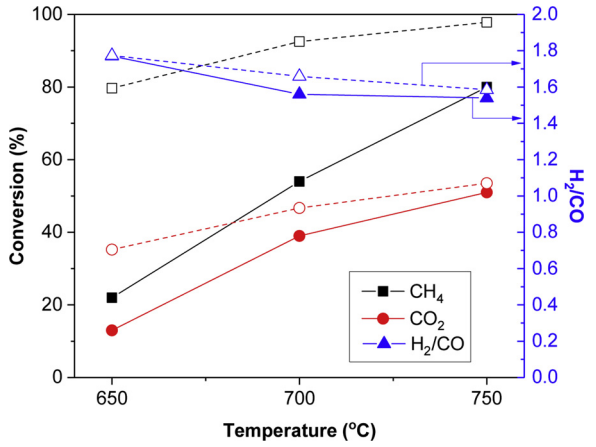


**Fig. 6.** Temperature effect on $CH_4$ and $CO_2$ conversions and $H_2/CO$ ratio ($CH_4/CO_2/H_2O$: 1/1/1, P = 1 atm, WHSV = 30 $L.g^{-1}.h^{-1}$). The thermodynamic equilibrium are plotted in dashes.

perovskite material which reflects the potential of this advanced catalyst for hydrogen-rich syngas production.

### 3.3.4. Temperature effect

The effect of temperature in BRM conditions was studied using a feed containing 25% of water and results are shown in Fig. 6. An increase in conversion is observed as the temperature increases as the thermodynamics predicts. At low temperature methane conversion is low and far away from equilibrium but as the temperature increases it gets closer to the equilibrium values and reaches a conversion of 80% at 750 °C. The low methane conversion at low temperature can be related to the high activation energy of $CH_4$. Methane needs high temperature to overcome the energy barrier necessary for its activation. Similarly to methane, $CO_2$ conversion is lower than the equilibrium at low temperature but gets closer to it as the temperature increases. At 750 °C, $CO_2$ conversion is only 2% below equilibrium reaching 51% conversion. In terms of selectivity, the $H_2/CO$ ratio follows the equilibrium trend and decreases slightly with the temperature.

## 3.4. Post-reaction characterisation

### 3.4.1. X-ray diffraction

The development of stable catalysts is one of the bottleneck for the implementation of combined reforming in commercial $CO_2$ conversion units. In this scenario, post reaction analysis is necessary to ascertain the robustness of our multicomponent catalyst under the studied reaction conditions. XRD was performed on the catalyst after reduction pretreatment and after reaction at 700 °C under DRM and BRM conditions to detect any structural changes induced to the catalyst. The resulting profiles are shown in Fig. 7. No structural changes were detected between the fresh catalyst (Fig. 1) and the reduced catalyst. The characteristic diffraction features of $La_2Zr_2O_7$ are still present attesting of the thermal stability of this material. No trace of metallic Ni was detected showing that either the reduced Ni particles are small and well dispersed or that Ni remains in the pyrochlore and double perovskite phases. Moreover the double perovskite phase $La_2NiZrO_6$ is still present and did not completely reduce to Ni, $La_2O_3$ and $ZrO_2$. After DRM and BRM reactions, a shoulder is detected at 44.4° and a small peak appears at 51.7°, corresponding to the main diffraction peaks of metallic Ni. The appearance of these peaks could be due to a certain degree of Ni sintering but also to the exsolution of Ni from the pyrochlore structure during reaction [26]. In view of the excellent performance with no deactivation observed during 24 h of continuous run the exsolution of Ni is plausible in agreement with previous reports [36]. In fact, the low surface area of the catalyst (Table S1, Supporting information) supports this claim as Ni is very small (around 21 nm after reaction, according to the Scherrer equation) and therefore must be well dispersed on the surface and possibly released from the structure as the reaction takes place. Traces of $La_2O_3$ (JCPDS Card No. 01-074-2430) are detected after reaction, resulting either from the partial decomposition of the pyrochlore or from the partial reduction of the double perovskite.

### 3.4.2. Temperature programmed oxidation

Carbon is a side product of $CO_2$-reforming reactions and is the main cause of catalyst deactivation. Carbonaceous species potentially formed on the catalyst were quantified and identified by temperature programmed oxidation. The $CO_2$ production profiles of samples that have undergone DRM and BRM with different amount of steam are shown in Fig. 8. This analysis shows that no carbon was formed on the catalyst when water was introduced into the system. Indeed under BRM conditions, carbon formation is minimised due to the reverse CO reduction reaction ($C_{(s)} + H_2O \rightarrow CO + H_2$). The presence of steam prevents the deactivation of the catalyst by carbon formation. However under DRM conditions (i.e. 0% water) a significant amount of carbon was formed ($0.01 g_C/g_{cat}$). Three different oxidation processes can be distinguished corresponding to different carbonaceous species. The low temperature peak at 270 °C is attributed to the gasification of $C_\alpha$ amorphous carbon. $C_\alpha$ are believed to be active species in reforming, originating from nickel carbide produced during methane decomposition [37]. The second peak at 445 °C corresponds to $C_\beta$ filament carbon. This type of carbon can be eliminated at relatively low temperature [38]. Finally,

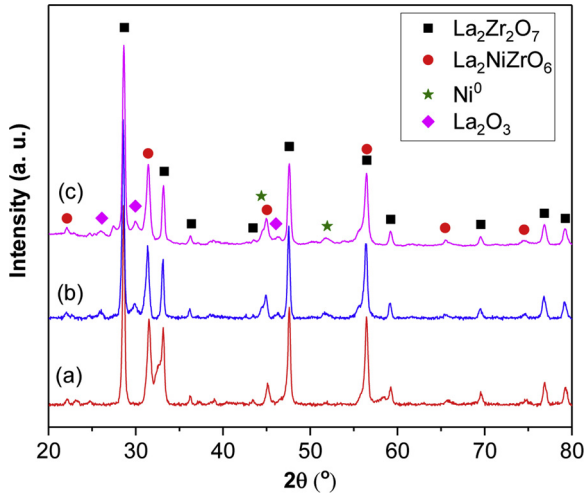


**Fig. 7.** XRD patterns of LNZ10 (a) reduced, (b) after DRM and (c) after BRM.

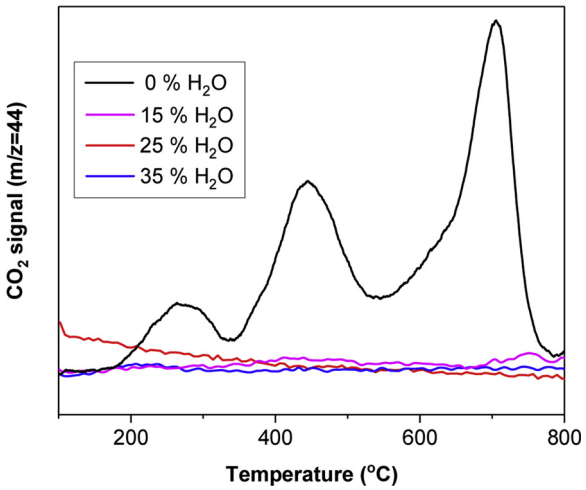


**Fig. 8.** TPO profiles of the catalysts after reaction at 700 °C and 60 $L.g^{-1}.h^{-1}$.

the third peak, at 705 °C, corresponds to the oxidation of more graphitic carbon, inert and requiring high temperature to remove. The later indicates that coking will be a factor to consider if our pyrochlore-perovskite catalysts are going to be used in a DRM unit. Nonetheless, the addition of water (BRM mode) heavily mitigates the impact of carbon deposition resulting in a stable catalyst to produce $H_2$-rich syngas streams. The Raman analysis presented in Figure S2 supports this claim. Experiments were conducted on the samples after reaction. No evidence of carbon species were found on the samples after BRM reaction. However the typical D and G bands of multiwall carbon nanotubes were observed at 1342 and 1576 cm-1 respectively on the sample after DRM.

## 4. Conclusions

This work provides evidence of the excellent performance of a Nickel-doped pyrochlore catalyst for chemical $CO_2$ recycling via DRM and BRM. Structural analysis revealed the presence of the pyrochlore and a secondary double perovskite phase which constitutes the basis of this novel catalyst. After the reaction, small Ni clusters are present on the surface of the catalyst as suggested by XRD and TPR. In fact, it is very likely that active Ni clusters are exsolved from the pyrochlore during BRM and DRM leading to highly dispersed active ensembles which account for the high activity and stability of the catalyst during both reactions. Very importantly, the $H_2$/CO ratio produced by the catalyst can be fine-tuned by introducing steam into the system, enabling a flexible syngas production for a variety of applications. Our engineered catalyst also allows adjustment of the syngas ratio under different reactions conditions such as temperature and space time, thus making it very versatile when process integration is considered. As an additional advantage, carbon deposition over the pyrochlore-perovskite catalyst is fully eliminated when steam is added to the reforming mixtures. Overall, this work showcases a strategy to design highly effective heterogeneous catalysts for gas-phase $CO_2$ valorisation – the stabilisation of Ni particles on a complex mixed oxide structure resulting in a powerful dry and bi-reforming catalyst able to deliver customised syngas for chemical synthesis.

## Acknowledgments

This work was supported by the Department of Chemical and Process Engineering at the University of Surrey and the EPSRC grant EP/R512904/1 as well as the Royal Society Research GrantRSGR1180353. This work was also partially sponsored by the CO2Chem through the EPSRC grant EP/P026435/1. The Ministerio de Economía, Industria y Competitividad of Spain (Project ENE2015-66975-C3-2-R) co-financed by FEDER funds from the European Union supported the work done in Spain. Finally, E. le Saché would like to acknowledge the Armourers & Brasiers Gauntlet Trust for their travel grant award.

## Appendix A. Supplementary data

Supplementary material related to this article can be found, in the online version, at doi:https://doi.org/10.1016/j.cattod.2019.05.039.

## References

[1] Global Energy and $CO_2$ Status Report - 2017, International Energy Agency, 2018.
[2] E.A. Quadrelli, G. Centi, J.L. Duplan, S. Perathoner, Carbon dioxide recycling: emerging large-scale technologies with industrial potential, ChemSusChem 4 (2011) 1194–1215.
[3] R.M. Cuéllar-Franca, A. Azapagic, Carbon capture, storage and utilisation technologies: a critical analysis and comparison of their life cycle environmental impacts, J. CO2 Util. 9 (2015) 82–102.
[4] G.A. Olah, A. Goeppert, M. Czaun, G.K.S. Prakash, Bi-reforming of methane from any source with steam and carbon dioxide exclusively to metgas (CO-2$H_2$) for methanol and hydrocarbon synthesis, J. Am. Chem. Soc. 135 (2013) 648.
[5] D. Pakhare, J. Spivey, A review of dry ($CO_2$) reforming of methane over noble metal catalysts, Chem. Soc. Rev. 43 (2014) 7813–7837.
[6] N.D. Charisiou, G. Siakavelas, K.N. Papageridis, A. Baklavaridis, L. Tzounis, D.G. Avraam, M.A. Goula, Syngas production via the biogas dry reforming reaction over nickel supported on modified with $CeO_2$ and/or $La_2O_3$ alumina catalysts, J. Nat. Gas Sci. Eng. 31 (2016) 164–183.
[7] A. Nakhaei Pour, M. Mousavi, Combined reforming of methane by carbon dioxide and water: particle size effect of Ni–Mg nanoparticles, Int. J. Hydrogen Energy 40 (2015) 12985–12992.
[8] J. Lachén, J. Herguido, J.A. Peña, Production and purification of hydrogen by biogas combined reforming and steam-iron process, Int. J. Hydrogen Energy (2018).
[9] A. Wolfbeisser, O. Sophiphun, J. Bernardi, J. Wittayakun, K. Föttinger, G. Rupprechter, Methane dry reforming over ceria-zirconia supported Ni catalysts, Catal. Today 277 (2016) 234–245.
[10] R. Chai, G. Zhao, Z. Zhang, P. Chen, Y. Liu, Y. Lu, High sintering-/coke-resistance Ni@$SiO_2$/$Al_2O_3$/FeCrAl-fiber catalyst for dry reforming of methane: one-step, macro-to-nano organization via cross-linking molecules, Catal. Sci. Technol. 7 (2017) 5500–5504.
[11] V.R. Choudhary, K.C. Mondal, A.S. Mamman, U.A. Joshi, Carbon-free dry reforming of methane to syngas over $NdCoO_3$ perovskite-type mixed metal oxide catalyst, Catal. Lett. 100 (2005) 271.
[12] M.C.J. Bradford, M.A. Vannice, $CO_2$ reforming of $CH_4$ over supported Ru catalysts, J. Catal. 183 (1999) 69–75.
[13] M.-S. Fan, A.Z. Abdullah, S. Bhatia, Catalytic technology for carbon dioxide reforming of methane to synthesis gas, ChemCatChem 1 (2009) 192–208.
[14] P. Boldrin, E. Ruiz-Trejo, J. Mermelstein, J.M. Bermúdez Menéndez, T. Ramírez Reina, N.P. Brandon, Strategies for carbon and sulfur tolerant solid oxide fuel cell materials, incorporating lessons from heterogeneous catalysis, Chem. Rev. 116 (2016) 13633–13684.
[15] S.M. de Lima, J.M. Assaf, Synthesis and characterization of $LaNiO_3$, $LaNi_{(1-x)}Fe_xO_3$ and $LaNi_{(1-x)}Co_xO_3$ perovskite oxides for catalysis application, Mat. Res. 5 (2002) 329–335.
[16] S. Dama, S.R. Ghodke, R. Bobade, H.R. Gurav, S. Chilukuri, Active and durable alkaline earth metal substituted perovskite catalysts for dry reforming of methane, Appl. Catal. B 224 (2018) 146–158.
[17] X. Zhang, X. Fang, X. Feng, X. Li, W. Liu, X. Xu, N. Zhang, Z. Gao, X. Wang, W. Zhou, Ni/$Ln_2Zr_2O_7$ (Ln = La, Pr, Sm and Y) catalysts for methane steam reforming: the effects of A site replacement, Catal. Sci. Technol. 7 (2017) 2729–2743.
[18] Y. Ma, X. Wang, X. You, J. Liu, J. Tian, X. Xu, H. Peng, W. Liu, C. Li, W. Zhou, P. Yuan, X. Chen, Nickel-supported on $La_2Sn_2O_7$ and $La_2Zr_2O_7$ pyrochlores for methane steam reforming: insight into the difference between tin and zirconium in the B site of the compound, ChemCatChem 6 (2014) 3366–3376.
[19] J.M. Sohn, M.R. Kim, S.I. Woo, The catalytic activity and surface characterization of $Ln_2B_2O_7$ (Ln = Sm, Eu, Gd and Tb; B = Ti or Zr) with pyrochlore structure as novel $CH_4$ combustion catalyst, Catal. Today 83 (2003) 289–297.
[20] R. Shukla, K. Vasundhara, P.S.R. Krishna, A.B. Shinde, S.K. Sali, N.K. Kulkarni, S.N. Achary, A.K. Tyagi, High temperature structural and thermal expansion behavior of pyrochlore-type praseodymium zirconate, Int. J. Hydrogen Energy 40 (2015) 15672–15678.
[21] S.-F. Weng, H.-C. Hsieh, C.-S. Lee, Hydrogen production from oxidative steam reforming of ethanol on nickel-substituted pyrochlore phase catalysts, Int. J. Hydrogen Energy 42 (2017) 2849–2860.
[22] D. Pakhare, D. Haynes, D. Shekhawat, J. Spivey, Role of metal substitution in lanthanum zirconate pyrochlores (La2Zr2$O_7$) for dry (CO2) reforming of methane (DRM), Appl. Petrochem. Res. 2 (2012) 27–35.
[23] N. Kumar, A. Roy, Z. Wang, E.M. L'Abbate, D. Haynes, D. Shekhawat, J.J. Spivey, Bi-reforming of methane on Ni-based pyrochlore catalyst, Appl. Catal. A Gen. 517 (2016) 211–216.
[24] N. Kumar, Z. Wang, S. Kanitkar, J.J. Spivey, Methane reforming over Ni-based pyrochlore catalyst: deactivation studies for different reactions, Appl. Petrochem. Res. 6 (2016) 201–207.
[25] T.R. Reina, E. le Saché, D. Watson, L. Pastor Perez, A. Sepulveda Escribano, Catalysts for the Reforming of Gaseous Mixtures, U.o. Surrey, UK, 2017.
[26] E. le Saché, L. Pastor-Pérez, D. Watson, A. Sepúlveda-Escribano, T.R. Reina, Ni stabilised on inorganic complex structures: superior catalysts for chemical $CO_2$ recycling via dry reforming of methane, Appl. Catal. B 236 (2018) 458–465.
[27] C. Wan, W. Zhang, Y. Wang, Z. Qu, A. Du, R. Wu, W. Pan, Glass-like thermal conductivity in ytterbium-doped lanthanum zirconate pyrochlore, Acta Mater. 58 (2010) 6166–6172.
[28] H. Chen, Y. Gao, Y. Liu, H. Luo, Coprecipitation synthesis and thermal conductivity of $La_2Zr_2O_7$, J. Alloys. Compd. 480 (2009) 843–848.
[29] K. Holliday, S. Finkeldei, S. Neumeier, C. Walther, D. Bosbach, T. Stumpf, TRLFS of $Eu^{3+}$ and $Cm^{3+}$ doped $La_2Zr_2O_7$: a comparison of defect fluorite to pyrochlore structures, J. Nucl. Phys. Mater. Sci. Radiat. Appl. 433 (2013) 479–485.
[30] F.W. Poulsen, M. Glerup, P. Holtappels, Structure, Raman spectra and defect chemistry modelling of conductive pyrochlore oxides, Solid State Ion. 135 (2000) 595–602.
[31] D.J. Haynes, D. Shekhawat, D.A. Berry, J. Zondlo, A. Roy, J.J. Spivey, Characterization of calcination temperature on a Ni-substituted lanthanum-strontium-zirconate pyrochlore, Ceram. Int. 43 (2017) 16744–16752.
[32] E. le Saché, J.L. Santos, T.J. Smith, M.A. Centeno, H. Arellano-Garcia, J.A. Odriozola, T.R. Reina, Multicomponent Ni-$CeO_2$ nanocatalysts for syngas production from $CO_2$/$CH_4$ mixtures, J. CO2 Util. 25 (2018) 68–78.
[33] V. Arcotumapathy, F.S. Alenazey, R.L. Al-Otaibi, D.-V.N. Vo, F.M. Alotaibi, A.A. Adesina, Mechanistic investigation of methane steam reforming over Ce-promoted Ni/SBA-15 catalyst, Appl. Petrochem. Res. 5 (2015) 393–404.
[34] K. Ahmed, K. Foger, Kinetics of internal steam reforming of methane on Ni/YSZ-

based anodes for solid oxide fuel cells, Catal. Today 63 (2000) 479–487.
[35] N. Laosiripojana, S. Assabumrungrat, Methane steam reforming over Ni/Ce–$ZrO_2$ catalyst: influences of Ce–$ZrO_2$ support on reactivity, resistance toward carbon formation, and intrinsic reaction kinetics, Appl. Catal. A Gen. 290 (2005) 200–211.
[36] O. Kwon, S. Sengodan, K. Kim, G. Kim, H.Y. Jeong, J. Shin, Y.-W. Ju, J.W. Han, G. Kim, Exsolution trends and co-segregation aspects of self-grown catalyst nanoparticles in perovskites, Nat. Commun. 8 (2017) 15967.
[37] M. Argyle, C. Bartholomew, Heterogeneous catalyst deactivation and regeneration: a review, Catalysts 5 (2015) 145.
[38] L. Zhou, L. Li, N. Wei, J. Li, J.-M. Basset, Effect of $NiAl_2O_4$ formation on Ni/$Al_2O_3$ stability during dry reforming of methane, ChemCatChem 7 (2015) 2508–2516.